

Prospects for detecting neutron star–white dwarf mergers with decihertz gravitational-wave observatories

Yacheng Kang,^{1,2} Chang Liu,^{1,2,3} Jin-Ping Zhu,^{4,5} Yong Gao,^{1,2,6} Lijing Shao,^{2,7}★ Bing Zhang,^{8,9}†
 Hui Sun,⁷ Yi-Han Iris Yin¹⁰, and Bin-Bin Zhang^{10,11,12}

¹Department of Astronomy, School of Physics, Peking University, Beijing 100871, China

²Kavli Institute for Astronomy and Astrophysics, Peking University, Beijing 100871, China

³Laboratoire des 2 Infinis - Toulouse (L2IT-IN2P3), Université de Toulouse, CNRS, UPS, F-31062 Toulouse Cedex 9, France

⁴School of Physics and Astronomy, Monash University, Clayton Victoria 3800, Australia

⁵Monash Centre for Astrophysics, School of Physics and Astronomy, Monash University, Clayton, VIC 3800, Australia

⁶Max Planck Institute for Gravitational Physics (Albert Einstein Institute), Am Mühlenberg 1, Potsdam 14476, Germany

⁷National Astronomical Observatories, Chinese Academy of Sciences, Beijing 100012, China

⁸Nevada Center for Astrophysics, University of Nevada, Las Vegas, NV 89154, USA

⁹Department of Physics and Astronomy, University of Nevada, Las Vegas, NV 89154, USA

¹⁰School of Astronomy and Space Science, Nanjing University, Nanjing 210093, China

¹¹Key Laboratory of Modern Astronomy and Astrophysics (Nanjing University), Ministry of Education, China

¹²Purple Mountain Observatory, Chinese Academy of Sciences, Nanjing 210023, China

Accepted XXX. Received YYY; in original form ZZZ

ABSTRACT

Based on different neutron star–white dwarf (NS-WD) population models, we investigate the prospects of gravitational-wave (GW) detections for NS-WD mergers, with the help of early warnings from two space-borne decihertz GW observatories, DO-Optimal and DECIGO. We not only give quick assessments of the GW detection rates for NS-WD mergers with the two decihertz GW detectors, but also report systematic analyses on the characteristics of GW-detectable merger events using the method of Fisher matrix. With a sufficient one-day early-warning time, the yearly GW detection number for DO-Optimal is in the range of $(1.5\text{--}1.9) \times 10^3$, while it is $(3.3\text{--}4.6) \times 10^4$ for DECIGO. More importantly, our results show that most NS-WD mergers can be localized with an uncertainty of $\mathcal{O}(10^{-2})$ deg². Given the NS-WD merger as a possible origin for a peculiar long-duration gamma-ray burst, GRB 211211A, followed with kilonova-like emissions, we further suggest that the GW early-warning detection would allow future electromagnetic telescopes to get prepared to follow-up transients after some special NS-WD mergers. Based on our analyses, we emphasize that such a feasible “wait-for” pattern can help to firmly identify the origin of GRB 211211A-like events in the future and bring excellent opportunities for the multimessenger astronomy.

Key words: gravitational waves – gamma-ray bursts – binaries: general

1 INTRODUCTION

The mergers of double-compact-object (DCO) systems have been explored extensively, both as progenitors of various electromagnetic (EM) transients and as gravitational wave (GW) sources. For example, binary white dwarfs (BWDs) are not only one of the most promising candidates of type Ia supernova (SN) progenitors (Livio & Mazzali 2018; Soker 2018; Wang 2018; Ruitter 2020), but are also expected to be the dominant GW sources by numbers in our Milky Way (MW) for the Laser Interferometer Space Antenna (LISA) mission¹ (Lamberts et al. 2018; Bayle et al. 2022; Amaro-Seoane et al. 2023). For compact binary mergers containing at least

one neutron star (NS), it has long been proposed that the mergers of binary neutron stars (BNSs) and neutron star–black holes (NS-BHs) are the progenitors of short-duration gamma-ray bursts (sGRBs; Paczynski 1986; Eichler et al. 1989; Narayan et al. 1992; Zhang 2018). The milestone co-detection of GW and EM signals during GW170817/GRB 170817A/AT 2017gfo events (Abbott et al. 2017a,b; Goldstein et al. 2017; Savchenko et al. 2017; Coulter et al. 2017; Evans et al. 2017; Pian et al. 2017; Kilpatrick et al. 2017; Zhang et al. 2018) has not only provided us a smoking-gun evidence for the BNS merger origin of sGRBs and kilonovae (Li & Paczynski 1998), but also an unprecedented opportunity to explore gravity theories and fundamental physics in extreme environments (Abbott et al. 2017c, 2018b, 2019; Shao et al. 2017; Sathyaprakash et al. 2019; Arun et al. 2022).

Nevertheless, the mergers of other kinds of DCO systems, such as NS-WD binaries, have not been explored to the same depth in literature. Until recently, Yang et al. (2022) adopted a NS-WD merger scenario to explain the kilonova-like emission following a peculiar

★ E-mail: lshao@pku.edu.cn

† E-mail: bing.zhang@unlv.edu

¹ LISA is an ESA-led space-borne GW observatory, with NASA as a junior partner. It is due to be launched in 2034 with the aim to record and study GWs in the millihertz frequency band. More information about the LISA mission can be found at <https://lisa.nasa.gov>.

long-duration gamma-ray burst (IGRB), GRB 211211A (Rastinejad et al. 2022; Troja et al. 2022; Mei et al. 2022; Gompertz et al. 2023), attracting significant attention on NS-WD mergers and their detection prospects (Zhong et al. 2023; Yin et al. 2023). Compared with other types of DCO systems (e.g., BWDs, BNSs, NS-BHs, etc.), the different component properties of NS-WD binaries could have significant impacts on the early-time dynamics of mass-transfer phase, initial conditions of accretion disk, and final merger remnants, etc. (King et al. 2007; Chattopadhyay et al. 2007; Paschalidis et al. 2011; Margalit & Metzger 2016, 2017). In particular, Zhong et al. (2023) showed that GRB 211211A-like events could arise from a NS-WD merger if the central engine leaves a magnetar behind. They proposed that the magnetic bubble eruptions from the toroidal magnetic field amplification of the pre-merger NS could successfully produce the main burst of GRB 211211A. NS-WD systems are likely the most common type of DCO systems besides BWDs (Nelemans et al. 2001b; Toonen et al. 2018), and may have various observable explosive transients (Metzger 2012; Zenati et al. 2019; Fernández et al. 2019; Gillanders et al. 2020; Bobrick et al. 2022; Kaltenborn et al. 2023), which will bring excellent opportunities for future multimessenger astronomy. Overall, it is worth analyzing the consequences of NS-WD mergers in more detail.

Based on the above arguments, in this work we discuss the realistic prospects of detecting NS-WD mergers with GW early warnings using space-borne decihertz GW detectors. Given the lower sensitive frequency range (0.01–1 Hz) of decihertz detectors, they can offer alerts to NS-WD mergers much earlier than the current and future ground-based detectors² (usually sensitive in the 10–10⁴ Hz band), or even earlier than the EM facilities (Liu et al. 2022b; Kang et al. 2022; Kang et al. 2023). In addition, another motivation to consider decihertz GW early warnings is that the upper cutoff GW frequency is expected to be $\lesssim 1$ Hz for NS-WD mergers in their inspiral phase. This is because the runaway mass-transfer phase and tidal disruption outcome occur earlier for NS-WD mergers (Verbunt & Rappaport 1988; Paschalidis et al. 2009; Margalit & Metzger 2016; Kaltenborn et al. 2023), especially when compared with BNS and NS-BH merger events.³ In view of this, it would be difficult for the NS-WD inspiral GW signals to enter the ground-based GW detectors, unlike the situation for more massive DCO systems. Nevertheless, it allows us to propose a feasible “wait-for” GW detecting mode for NS-WD mergers with decihertz GW detectors, and provide helpful inputs for future multimessenger astrophysics.

Before quantitatively analysing the early warnings from two representative decihertz GW observatories, DO-Optimal (DO-OPT; Sedda et al. 2020, 2021) and DECIGO (DEC; Kawamura et al. 2011, 2021), we first use the method of convolution with different star formation rates (SFRs) and delay-time distributions (DTDs) to obtain four kinds of NS-WD merger population models. Given the short tidal-disruption timescale (see, e.g., Kaltenborn et al. 2023), $\lesssim O(\text{min})$, and possibly observable EM transients (King et al. 2007; Chattopadhyay et al. 2007; Metzger 2012; Margalit & Metzger 2016, 2017; Yang et al. 2022) for NS-WD mergers, we follow Kang et al. (2022)

and set the early-warning time to be $t_e = 1$ d and signal-to-noise ratio (SNR) threshold value to be 8 for our GW detection strategy. Differently from BNS mergers or NS-BH mergers, we define the time when the WD starts to experience the Roche-lobe overflow as the merger time for NS-WD binaries, considering that there is no well-modeled GW waveform during the runaway mass-transfer phase. With the aim to extend early studies on decihertz GW alerts for NS-WD mergers, we not only give quick assessments of yearly detection numbers and percentages with DO-OPT and DEC, but also report more detailed analyses on the characteristics of GW-detectable merger events using the Fisher matrix. We find that DEC has better performance than DO-OPT as a whole on GW early-warning detections and localization abilities, especially for high-redshift (high- z) events. For those mergers that would yield the best estimation results of distance and angular resolution, we collect them into a Golden Sample Set, and present the detection rates of NS-WD mergers in the Golden Sample Set for different population models with DO-OPT and DEC.

Taking the recent peculiar IGRB, GRB 211211A, as an example, we further suggest that the GW early-warning detection would allow future EM telescopes to get prepared for possible follow-up transients after some special NS-WD mergers. Although there are a few groups suggesting different origins for GRB 211211A,⁴ at least most studies have supported or directly considered compact star merger scenarios for this event, namely compact-binary IGRBs (cb-IGRBs), given the features of kilonova-like emissions and host-galaxy properties including the offset, etc.. Regardless of the exact composition of this binary system, with a sufficient early-warning time ($t_e = 1$ d) and localization accuracies ($\Delta\Omega \lesssim 1 \text{ deg}^2$), we point out that one can prepare well in advance for future EM transients of GRB 211211A-like events, and no longer needs to consider the field of view (FoV) discounts and complex searching strategies.⁵ Such a feasible wait-for pattern, if realized in future, can help to firmly identify the origin of GRB 211211A-like events and enhance the comprehension of GRB’s physical type.

The organization of this paper is as follows. We first overview the construction of the NS-WD merger population models in Section 2. In Section 3, we introduce the GW detecting strategy with two space-borne decihertz GW observatories. Using the above ingredients, we report our results and detailed analyses on GW early-warning detections of NS-WD mergers in Section 4. Finally, Section 5 concludes the paper. Throughout this paper, we adopt a standard Λ CDM model with the matter density parameter $\Omega_m = 0.315$, the dark-energy density parameter $\Omega_\Lambda = 0.685$, and the Hubble-Lemaître constant $H_0 = 67.4 \text{ km s}^{-1} \text{ Mpc}^{-1}$ (Aghanim et al. 2020).

² Ground-based GW detectors include the current Advanced Laser Interferometer Gravitational-wave Observatory (LIGO), the Advanced Virgo, the Kamioka Gravitational Wave Detector (KAGRA), and the future next-generation detectors, such as the Einstein Telescope and the Cosmic Explorer (Abbott et al. 2018a; Reitze et al. 2019; Maggiore et al. 2020; Ronchini et al. 2022; Banerjee et al. 2023; Branchesi et al. 2023).

³ Note that for BNS and NS-BH mergers in the inspiral phase, the upper cutoff GW frequency can be approximated by the GW frequency at the innermost stable circular orbit.

⁴ For examples, Waxman et al. (2022) have shown that the thermal emission from dust could explain the observed near-infrared data; Zhu et al. (2022c) have suggested that a NS-BH merger could roughly reproduce the multi-wavelength observations; Gompertz et al. (2023) concluded that the spectral evolution could be explained by a transition from a fast-cooling mode to a slow-cooling regime, favoring a BNS merger scenario rather than a NS-BH origin; Barnes & Metzger (2023) also found that the afterglow-subtracted emission of GRB 211211A is in best agreement for collapsar models with high kinetic energies. Unfortunately, GRB 211211A was detected prior to the fourth observing run of the LIGO-Virgo-KAGRA Collaboration. Overall, the origin of GRB 211211A is still under debate.

⁵ We refer readers to Kang et al. (2022) for more descriptions.

Table 1. Simulated NS-WD merger numbers per year for different population models with $\dot{\rho}_0 = 390 \text{ Gpc}^{-3} \text{ yr}^{-1}$. In the last row, we list the lower and upper values in brackets, by rescaling our results with $\dot{\rho}_0 \approx [90, 5800] \text{ Gpc}^{-3} \text{ yr}^{-1}$. More descriptions of the four population models are given in Section 2.1.

| Population Model | | | |
|---------------------------------------|---------------------------------------|---------------------------------------|---------------------------------------|
| A | B | C | D |
| 5.6×10^5 | 4.1×10^5 | 4.9×10^5 | 3.8×10^5 |
| $(1.3 \times 10^5 - 8.3 \times 10^6)$ | $(9.5 \times 10^4 - 6.1 \times 10^6)$ | $(1.1 \times 10^5 - 7.4 \times 10^6)$ | $(8.7 \times 10^4 - 5.6 \times 10^6)$ |

2 NS-WD POPULATION

In this section, we briefly describe how we obtain the NS-WD populations prepared for later analyses. Following Sun et al. (2015), we also ignore the possible redshift evolution of intrinsic system parameters for NS-WD mergers. Within this framework, one can separately discuss the redshift distribution of NS-WD systems in Section 2.1. We show more details about mass distribution of our NS-WD populations in Section 2.2.

2.1 Event rate and redshift distribution

The number density per unit time for NS-WD mergers at a given redshift z can be estimated as,

$$\frac{d\dot{N}}{dz} = \frac{\dot{\rho}_0 f(z)}{1+z} \frac{dV(z)}{dz}, \quad (1)$$

where $\dot{\rho}_0$ is the local NS-WD merger rate density, $f(z)$ is the dimensionless redshift distribution factor, and $\frac{dV(z)}{dz}$ is the comoving volume element,

$$\frac{dV(z)}{dz} = \frac{c}{H_0} \frac{4\pi D_L^2}{(1+z)^2 \sqrt{\Omega_\Lambda + \Omega_m(1+z)^3}}, \quad (2)$$

where c is the speed of light, and D_L is the luminosity distance,

$$D_L = (1+z) \frac{c}{H_0} \int_0^z \frac{dz}{\sqrt{\Omega_\Lambda + \Omega_m(1+z)^3}}. \quad (3)$$

The function $f(z)$ in Equation (1) depends on the DTD of NS-WD mergers superposed on the SFR. Considering different combinations of SFRs and DTDs, we illustrate in Appendix A the redshift distributions of $f(z)$ with more details. We consider two kinds of analytical models from Yuksel et al. (2008) and Madau & Dickinson (2014) for SFRs, abbreviated as ‘Y08’ and ‘MD14’, respectively; as for DTDs, two models—abbreviated as ‘ $\gamma\alpha$ -H’ and ‘ $\gamma\alpha$ -V’—are adopted in this work (see Appendix A for more descriptions). The population models are briefly summarized as follows:

- (1) **Model A:** Y08 + $\gamma\alpha$ -H;
- (2) **Model B:** Y08 + $\gamma\alpha$ -V;
- (3) **Model C:** MD14 + $\gamma\alpha$ -H;
- (4) **Model D:** MD14 + $\gamma\alpha$ -V.

For the local NS-WD merger rate density, we adopt $\dot{\rho}_0 = 390 \text{ Gpc}^{-3} \text{ yr}^{-1}$ from Zhao et al. (2021b) as the fiducial value, which is in agreement with many studies (Nelemans et al. 2001a; Kim et al. 2004; O’Shaughnessy & Kim 2010; Bobrick et al. 2017; Toonen et al. 2018). Moreover, in a similar way to that in Liu et al. (2022b), we will rescale our results in later sections by adjusting $\dot{\rho}_0$ in the range of $[8, 500] \text{ Myr}^{-1}$ per MW-like Galaxy, corresponding to $\dot{\rho}_0 \approx [90, 5800] \text{ Gpc}^{-3} \text{ yr}^{-1}$ hereafter (Kaltenborn et al. 2023).⁶

⁶ In most recent studies, a few authors obtained the conversion factor with

We regard this as a crude but reasonable treatment to assess the systematic uncertainties in our predictions. The simulated NS-WD merger rates in the Universe for different population models are listed in Table 1.

2.2 Mass distribution of NS-WD binaries

The mass distribution of NS-WD systems is a key ingredient in our calculation of GW detection rates. However, it is difficult to construct an analytical model for the probability density function of the component masses in NS-WD binaries. Therefore, for simplicity, we make use of the population-synthesis simulation results obtained by Kaltenborn et al. (2023). Given that there are two strong peaks in the mass distribution of NSs at $M_{\text{NS}} = 1.11 M_\odot$ and $M_{\text{NS}} = 1.26 M_\odot$ (see Figure 1 in Kaltenborn et al. 2023), we assume that each NS-WD merger may have $M_{\text{NS}} = 1.11 M_\odot$ or $M_{\text{NS}} = 1.26 M_\odot$ with an equal probability. The former is referred to as ‘Case I’, and the latter corresponds to ‘Case II’. In each case, without considering the detailed properties of NS-WD systems (e.g., the WD composition, the DTD models, etc.),⁷ we choose to fit the mass distribution of WD components using a model composed of multi-Gaussian components,

$$f_{\text{M}}^{\text{I}} \propto \left\{ a_1 \exp \left[-\frac{(M_{\text{WD}} - \mu_1)^2}{2\sigma_1^2} \right] + a_2 \exp \left[-\frac{(M_{\text{WD}} - \mu_2)^2}{2\sigma_2^2} \right] + a_3 \exp \left[-\frac{(M_{\text{WD}} - \mu_3)^2}{2\sigma_3^2} \right] \right\}, \quad (4)$$

and

$$f_{\text{M}}^{\text{II}} \propto \left\{ a_4 \exp \left[-\frac{(M_{\text{WD}} - \mu_4)^2}{2\sigma_4^2} \right] + a_5 \exp \left[-\frac{(M_{\text{WD}} - \mu_5)^2}{2\sigma_5^2} \right] \right\}. \quad (5)$$

Note that in the above equations, the WD component mass M_{WD} is in units of M_\odot . We plot the distribution of M_{WD} for Case I and Case II in Figure 1. The best-fit values of each parameter in Equation (4)

the galactic blue luminosity of $1.7 \times 10^{10} L_{\text{B},\odot}$ (Kalogera et al. 2001) and the blue luminosity for the local Universe of $1.98 \times 10^8 L_{\text{B},\odot} \text{ Mpc}^{-3}$ (Kopparapu et al. 2008), where $L_{\text{B},\odot} = 2.16 \times 10^{33} \text{ erg s}^{-1}$ is the Solar luminosity in the B-band.

⁷ This treatment is acceptable because Toonen et al. (2018) have suggested that there is no significant evolution of the average WD mass with the delay time for NS-WD binaries. We also find that the fractions of NS-WD mergers with different WD components (i.e., CO, ONe or He WDs) remain almost unchanged when different DTD models are adopted (see Table 2 in Toonen et al. 2018). Moreover, fractions shown in Kaltenborn et al. (2023) are also remarkably consistent with the results in Toonen et al. (2018).

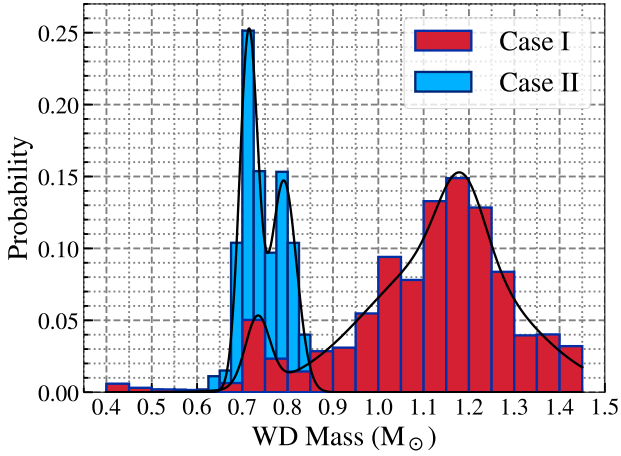


Figure 1. Distributions of the WD component mass obtained by [Kaltenborn et al. \(2023\)](#) for Case I (red) and Case II (blue). With the parameters given in Section 2.2, we also plot the best-fit lines (black) for each case. Note that here we have considered $M_{\text{WD}} \lesssim M_{\text{ch}}$, where $M_{\text{ch}} \approx 1.45 M_{\odot}$ is the Chandrasekhar mass limit.

and Equation (5) are

$$a_1 = 0.048, \quad \mu_1 = 0.73, \quad \sigma_1 = 0.027, \quad (6)$$

$$a_2 = 0.061, \quad \mu_2 = 1.18, \quad \sigma_2 = 0.051, \quad (7)$$

$$a_3 = 0.094, \quad \mu_3 = 1.14, \quad \sigma_3 = 0.17, \quad (8)$$

and

$$a_4 = 0.25, \quad \mu_4 = 0.71, \quad \sigma_4 = 0.020, \quad (9)$$

$$a_5 = 0.15, \quad \mu_5 = 0.79, \quad \sigma_5 = 0.028. \quad (10)$$

Finally, let us elaborate on the meaning of ‘merger’ for NS-WD systems in this work. Regardless of the evolution history, once a NS-WD binary is formed, it keeps losing its orbital energy through GW emission, causing the orbit to shrink. When GW emission drives the NS-WD system to the Roche-lobe overflow (RLOF) orbital separation, the mass from the WD begins to transfer to the NS companion. A well-known fit of the RLOF separation is given by ([Eggleton 1983](#)),

$$a_{\text{RLOF}} \approx R_{\text{WD}} \frac{0.6q^{2/3} + \ln(1 + q^{1/3})}{0.49q^{2/3}}, \quad (11)$$

where $q = M_{\text{WD}}/M_{\text{NS}}$ and R_{WD} is the WD radius. The latter can be well approximated by ([Nauenberg 1972](#)),

$$R_{\text{WD}} \approx 10^9 \text{ cm} \left(\frac{M_{\text{WD}}}{0.7 M_{\odot}} \right)^{-1/3} \left[1 - \left(\frac{M_{\text{WD}}}{M_{\text{ch}}} \right)^{4/3} \right]^{1/2}, \quad (12)$$

where $M_{\text{ch}} \approx 1.45 M_{\odot}$ is the Chandrasekhar mass limit assuming the mean molecular weight per electron, $\mu_e = 2$.

During the mass-transfer phase, the binary separation can increase due to the conservation of angular momentum; on the other hand, the WD radius increases due to its mass loss [see Equation (12)], which can increase the critical RLOF separation [i.e., a_{RLOF} in Equation (11)]. The competition between the two effects can result in different evolution processes. If a_{RLOF} grows much faster, the NS-WD system will quickly progress into runaway mass transfer, tidally disrupting the WD on a dynamical time-scale. Otherwise, the NS-WD system can maintain its stable mass transfer for a longer time. Many studies have found that the stability of mass transfer depends heavily on the mass ratio q ([Verbunt & Rappaport 1988](#); [Paschalidis et al. 2009](#); [Margalit & Metzger 2016](#)). They suggest that the mass transfer

is unstable for binaries with $q_{\text{crit}} \gtrsim 0.43\text{--}0.53$.⁸ Combined with the distribution of M_{WD} in our consideration (see Figure 1), it is safe to say that most NS-WD systems would finally have a runaway mass-transfer phase, rather than the stable mass transfer. Given that there is no well-modeled GW waveform for the NS-WD system during the runaway mass-transfer phase, we define the time when the WD starts to experience the RLOF as the merger time. We regard this as a reasonable treatment, especially considering the short tidal-disruption timescale, $\lesssim O(\text{min})$ (see, e.g., [Kaltenborn et al. 2023](#)) and possibly observable explosive outcomes for NS-WD mergers ([King et al. 2007](#); [Chattopadhyay et al. 2007](#); [Metzger 2012](#); [Margalit & Metzger 2016, 2017](#); [Yang et al. 2022](#); [Zhong et al. 2023](#)). Note that such definitions would be very different from those in BNS and NS-BH mergers in many studies ([Kyutoku et al. 2011](#); [Shibata & Taniguchi 2011](#); [Zhu et al. 2021](#); [Liu & Shao 2022](#); [Liu et al. 2022b](#)). Essentially, for the NS-WD mergers in this work, the GW early-warning detections are actually to offer alerts on the RLOF time. For this reason, we will only consider the GW signal detectability in the inspiral phase, when the NS and WD can be regarded as well-separated bodies that gradually spiral towards one another. More descriptions of GW early-warning detections are presented in Section 3.

3 GW DETECTION STRATEGY

As mentioned in the Introduction, due to the higher sensitive frequency range of the ground-based GW detectors, they cannot offer alerts as early as the GW detectors in the decihertz band. Moreover, for space-borne decihertz GW detectors, NS-WD signals can exist from the start of the mission to their mergers or even to the end of the mission. Therefore, such GW signals will exist in decihertz detectors long enough to guarantee a relatively stable parameter estimation precision, especially for the localization. This means that the decihertz GW detectors can provide early-warning alerts to other GW and EM detectors for follow-ups. Following [Liu et al. \(2022b\)](#), our realistic detection strategy is performed as follows. Note that we use geometric units where $G = c = 1$ in this section.

Throughout this paper, we mainly compare the performance on GW early warnings between two space-borne decihertz GW detectors, DO-OPT and DEC. DO was envisaged in the ESA’s Voyage 2050 call ([Sedda et al. 2020, 2021](#)), where DO-OPT is the one with more ambitious LISA-like designs. DEC is a future Japanese space-borne decihertz GW mission with four independent LISA-like detectors ([Kawamura et al. 2011, 2021](#)). Parameters of the two detectors are available in, e.g., [Liu & Shao \(2022\)](#). In the community, there are more proposed decihertz detectors, including atom-interferometer-based detectors ([Zhao et al. 2021a](#); [Baum et al. 2023](#)) and moon-based ones ([Jani & Loeb 2021](#); [Harms et al. 2021](#); [Li et al. 2023](#); [Shao 2023](#)). In comparison, the sensitivity curves of DO-OPT and DEC are expected to perform much better than these mentioned detectors in the decihertz band.

We define t_{c_0} as the NS-WD’s time to merge since the start of the observation with decihertz GW detectors. To obtain the yearly detection rates, we only use early-warning NS-WD samples that will merge in 1–2 yr since the mission begins (e.g., $1 \text{ yr} \leq t_{\text{c}_0} \leq 2 \text{ yr}$). The sources that merge within 1 yr ($t_{\text{c}_0} < 1 \text{ yr}$) are discarded. This

⁸ [Bobrick et al. \(2017\)](#) have recently suggested that winds from the accreting stream are far more important to the stability, which brings a much smaller $q_{\text{crit}} \gtrsim 0.20$. Note that such a lower q_{crit} value is also in line with the results in [Kaltenborn et al. \(2023\)](#).

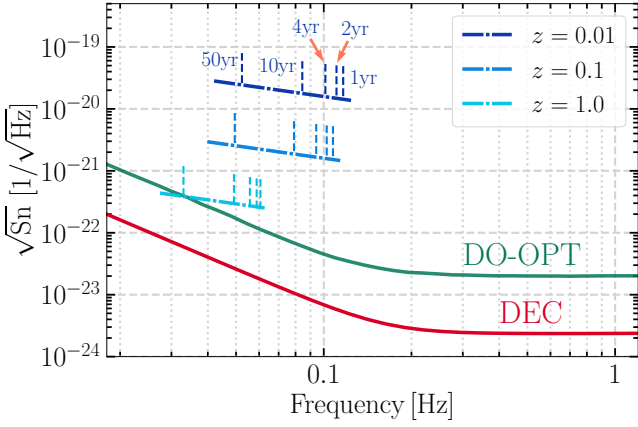


Figure 2. Sensitivity curves of DO-OPT (green) and DEC (red). The simulated NS-WD inspiral signals at different redshifts are plotted with blue dashed-dotted lines. Taking $M_{\text{NS}} = M_{\text{WD}} = 1.1 M_{\odot}$ as an example, source signals are plotted with a duration of ~ 100 yr. For each source, the short dashed vertical lines mark the time before RLOF occurs (i.e., the rightmost endpoint). More descriptions of the sky-averaged effective noise $\sqrt{S_n}$ for various detectors can be found in Liu et al. (2020).

is because their GW signals only stay shortly in the decihertz detectors, and not enough information is accumulated to obtain precise parameter estimations. Liu et al. (2022b) have shown that decihertz detectors have poor performances for BNSs that merge within 1 yr, which also applies to our NS-WD mergers. Considering that NS-WD mergers typically produce signals at around 0.1 Hz, there will only be a slight frequency chirp effect in the decihertz band (see Figure 2). This means that the choice of the maximum value of t_{c_0} will have minor effects on the yearly detection results as long as it is not too long.⁹ The above discussions explain why we only consider NS-WD mergers with $1 \text{ yr} \leq t_{c_0} \leq 2 \text{ yr}$.

Following Liu et al. (2022b), we generate NS-WD mergers weekly according to the population models. Then we calculate their SNRs. If $\text{SNR} > 8$, we claim the detection and calculate parameter precisions using the Fisher matrix (Finn 1992; Cutler & Flanagan 1994). As a fast way to estimate parameter statistical errors, a Fisher information matrix (FIM) shows the Cramer–Rao bound of parameters. In other words, a FIM tells us how precisely we can determine the model parameters for events with a high SNR and Gaussian noises (see Wang et al. (2022) for extensions of the FIM). Note that the choice of SNR threshold may vary depending on the specific goals of a study, which deserves more detailed analyses. We follow the settings in Liu & Shao (2022) with slight revisions. In total nine system parameters are used in the FIM, collectively denoted as

$$\Xi = \{M_z, \eta, t_c, \phi_c, D_L, \bar{\theta}_S, \bar{\phi}_S, \bar{\theta}_L, \bar{\phi}_L\}. \quad (13)$$

In Ξ , $\eta \equiv M_{\text{NS}}M_{\text{WD}}/(M_{\text{NS}} + M_{\text{WD}})^2$ is the symmetric mass ratio for each NS-WD merger system; $M_z \equiv (1+z)(M_{\text{NS}} + M_{\text{WD}})\eta^{3/5}$ is the detector-frame chirp mass; t_c and ϕ_c are the time and orbital phase at coalescence, respectively; and $\{\bar{\theta}_S, \bar{\phi}_S, \bar{\theta}_L, \bar{\phi}_L\}$ are the source direction and angular momentum direction in the Solar system

⁹ Note that people usually set a 4-yr mission time for DO-OPT and DEC. For sources that only inspiral within the whole 4-yr observational span (e.g., $t_{c_0} > 4$ yr), Liu et al. (2022b) have shown that their timing accuracies have a sharp decreasing trend, which is unfavorable for GW early-warning detections. In contrast, sources with $1 \text{ yr} \leq t_{c_0} \leq 4$ yr are in general distributed uniformly in time (see Table 1 in Liu et al. 2022b).

barycentric frame (see Figure 1 in Liu et al. 2020). Note that in generating sources, we adopt $\cos \theta_S \in \mathcal{U}(-1, 1)$, $\cos \theta_L \in \mathcal{U}(-1, 1)$, $\phi_S \in \mathcal{U}(0, 2\pi)$, and $\phi_L \in \mathcal{U}(0, 2\pi)$, where $\mathcal{U}(\cdot, \cdot)$ denotes a uniform distribution.

After performing the FIM calculation, we obtain the angular resolution $\Delta\Omega$ via (Cutler 1998; Barack & Cutler 2004),

$$\Delta\Omega = 2\pi\sqrt{(\Delta\bar{\mu}_S\Delta\bar{\phi}_S)^2 - \langle\delta\bar{\mu}_S\delta\bar{\phi}_S\rangle^2}, \quad (14)$$

where $\Delta\bar{\mu}_S$ and $\Delta\bar{\phi}_S$ are the root-mean-square errors of $\bar{\mu}_S$ and $\bar{\phi}_S$ with $\bar{\mu}_S \equiv \cos \theta_S$, and $\langle\delta\bar{\mu}_S\delta\bar{\phi}_S\rangle$ is the covariance of $\bar{\mu}_S$ and $\bar{\phi}_S$. In this work, our attention focuses on the estimations of $\Delta\Omega$ and ΔD_L .

For the FIM in the frequency domain, we follow Kang et al. (2022) with slight revisions. We set the integration limit to be f_{in} and f_{out} . In an idealized setting of two point particles, assuming a circular Keplerian orbit with quadrupolar GW damping, the GW frequency will formally diverge at a finite value of time, t_{div} . However, for a real NS-WD system, we have noted previously in Section 2.2 that the merger time t_{c_0} corresponds to the time when the WD starts to experience the RLOF. Thus the upper cutoff GW frequency in this work is actually at the critical RLOF separation, which can be calculated, to a sufficient precision, by Kepler’s third law,

$$f_{\text{max}} \simeq \frac{1}{\pi(1+z)}\sqrt{\frac{M_{\text{NS}} + M_{\text{WD}}}{a_{\text{RLOF}}^3}}. \quad (15)$$

Note that the $(1+z)$ factor is included in the denominator due to the cosmological time dilation. With a known f_{max} value for each NS-WD system, we can then calculate the remaining time to divergence (Maggiore 2008),

$$t_{\text{RLOF}} = t_{\text{div}} - t_{c_0} = 5M_z^{-5/3}(8\pi f_{\text{max}})^{-8/3}. \quad (16)$$

For a NS-WD system to merge in time t_{c_0} , we thus have

$$f_{\text{in}} = [(t_{c_0} + t_{\text{RLOF}})/5]^{-3/8}M_z^{-5/8}/8\pi, \quad (17)$$

$$f_{\text{out}} = [(t_e + t_{\text{RLOF}})/5]^{-3/8}M_z^{-5/8}/8\pi, \quad (18)$$

with t_e the early-warning time before the merger. The early-warning time t_e is remarkably significant to the GW early-warning detections of NS-WD mergers, given the short tidal-disruption timescale and possibly observable EM transients during the runaway mass-transfer phase. We will present the results with $t_e = 1$ d in detail. More descriptions of the GW waveform construction and parameter estimation method were discussed in Liu & Shao (2022).

Finally, a word on the tidal deformability included in our GW waveform. At the late stages of the inspiral, the quadrupolar tidal field \mathcal{E}_{ij} of one compact component would induce a quadrupole moment Q_{ij} to the other. To the leading order in the adiabatic approximation, \mathcal{E}_{ij} and Q_{ij} are related by a linear response function, $Q_{ij} = -\lambda\mathcal{E}_{ij}$, where λ is the tidal Love number (Hinderer 2008). The static tidal effect enters the GW phase at the 5-th post-Newtonian order¹⁰ through the dimensionless binary tidal deformability $\tilde{\Lambda}$ (Flanagan & Hinderer 2008; Hinderer 2008; Favata 2014),

$$\tilde{\Lambda} = \frac{16(M_{\text{NS}} + 12M_{\text{WD}})M_{\text{NS}}^4\Lambda_{\text{NS}} + (M_{\text{WD}} + 12M_{\text{NS}})M_{\text{WD}}^4\Lambda_{\text{WD}}}{13(M_{\text{NS}} + M_{\text{WD}})^5}, \quad (19)$$

where Λ_{NS} and Λ_{WD} correspond respectively to the dimensionless

¹⁰ Post-Newtonian order represents the power of velocity squared relative to the leading Newtonian order for point-particle binary motion.

Table 2. Yearly detection numbers and percentages (in brackets) of NS-WD mergers for different population models with DO-OPT and DEC. We assume an early-warning time $t_e = 1$ d. The SNR threshold is set to be 8. Note that we only list results with $\dot{\rho}_0 = 390 \text{ Gpc}^{-3} \text{ yr}^{-1}$. Readers can rescale in the way as for the total simulated numbers in Table 1.

| GW Detector | Population Model | | | |
|-------------|-------------------|-------------------|-------------------|-------------------|
| | A | B | C | D |
| DO-OPT | 1915 (0.34 %) | 1637 (0.40 %) | 1722 (0.35 %) | 1489 (0.40 %) |
| DEC | 46049 (8.25 %) | 36134 (8.75 %) | 41272 (8.34 %) | 33314 (8.86 %) |

tidal deformability of the NS and the WD in a NS-WD binary system. With $\Lambda_{\text{WD}} \gg \Lambda_{\text{NS}}$ ¹¹ we can simplify Equation (19) to

$$\tilde{\Lambda} \approx \frac{(M_{\text{WD}} + 12M_{\text{NS}}) M_{\text{WD}}^4 \Lambda_{\text{WD}}}{(M_{\text{NS}} + M_{\text{WD}})^5}. \quad (20)$$

We follow [Wolz et al. \(2020\)](#) to obtain Λ_{WD} via the universal relation,

$$\ln \Lambda_{\text{WD}} = 2.02942 + 2.48377 \ln \bar{I}_{\text{WD}}, \quad (21)$$

where $\bar{I}_{\text{WD}} = I_{\text{WD}}/M_{\text{WD}}^3$ is the dimensionless moment of inertia of the WD, which can be calculated with another fitting universal relation,

$$\begin{aligned} \ln \bar{I}_{\text{WD}} = & 24.7995 - 39.0476 \left(\frac{M_{\text{WD}}}{1 M_{\odot}} \right) + 95.9545 \left(\frac{M_{\text{WD}}}{1 M_{\odot}} \right)^2 \\ & - 138.625 \left(\frac{M_{\text{WD}}}{1 M_{\odot}} \right)^3 + 98.8597 \left(\frac{M_{\text{WD}}}{1 M_{\odot}} \right)^4 - 27.4 \left(\frac{M_{\text{WD}}}{1 M_{\odot}} \right)^5. \end{aligned} \quad (22)$$

Note that although many theoretical studies have discussed the effects of mass transfer and dynamical tides for WDs ([Lai 2012](#); [Kremer et al. 2017](#); [Tauris 2018](#); [McNeill et al. 2020](#); [Kuns et al. 2020](#); [Lau et al. 2022](#)), there are still many uncertainties and unsettled problems, especially on the GW waveform construction with mass transfer. In addition, many studies have focused on the low-mass WD donors (i.e., He WDs) or BWD systems, which can be different from NS-WD binaries in our consideration. In the following sections, we mainly focus on the estimation of the accuracy of distance ΔD_L and angular resolution $\Delta\Omega$. These two quantities can be extracted from the inspiral chirp signal alone. We leave other complex effects involving WDs for future studies.

4 RESULT

In Table 2 we first summarize yearly detection numbers of NS-WD mergers for the four population models with DO-OPT and DEC. We also list corresponding percentages in brackets, showing the ratio to the total number of yearly simulated NS-WD mergers (cf Table 1). The SNR threshold is set to 8. Combining all the results shown in Table 2, we conclude that DEC performs much better than DO-OPT on GW early-warning detections as a whole, with the yearly detection number in the range of $\sim (3.3\text{--}4.6) \times 10^4$. The detection number for

DO-OPT is in the range of $\sim (1.5\text{--}1.9) \times 10^3$, which is approximately 20 times fewer than DEC. Given that DEC has a lower noise level (see Figure 2), it is reasonable for DEC to show better detection abilities, especially for detection at higher redshift, which is clearly shown in Figure 3. Taking the population Model A as an example, Figure 3 shows that DO-OPT can detect early-warning sources up to $z \lesssim 1.7$, while DEC could reach $z \lesssim 7.6$. Moreover, the detectable NS-WD mergers for DEC are clustered at $z \approx 0.8$, consistent with the peak of the redshift factor $f(z)$ for the population Model A (see Figure A1). In comparison, due to its limited detection abilities, most detectable NS-WD mergers for DO-OPT are clustered around $z \approx 0.25$, which is much closer than those of DEC. Similarly, for the maximum SNR value, Figure 3 shows that DEC could reach $\text{SNR} \approx 650$, while DO-OPT only reaches $\text{SNR} \approx 75$.

As mentioned in Section 3, GW early-warning detections of NS-WD mergers are essentially to offer alerts on the RLOF time. Assuming an early-warning time $t_e = 1$ d¹² for each NS-WD merger event, we calculate the integration upper limit f_{out} with the known f_{max} at the critical RLOF separation. We plot in Figure 4 the distributions of f_{out} for detectable NS-WD mergers observed by DO-OPT and DEC. Different colours correspond to different population models. As clearly shown in Figure 4, the majority of total detectable NS-WD mergers for DEC would cluster at $f_{\text{out}} \approx 0.1$ Hz. In comparison, the peak of f_{out} distribution for DO-OPT would be a little higher in a wider range (0.16–0.25 Hz). These could be explained by the cosmological redshift effect, given that DEC detect more high- z events.

Furthermore, based on the GW early-warning NS-WD mergers, we now present estimations for the accuracy of distance (ΔD_L) and angular resolution ($\Delta\Omega$), which will be of great use to synergy observations with EM facilities. As described in Section 3, our analyses are performed using the FIM method. We first compare $\Delta D_L/D_L$ - $\Delta\Omega$ distributions of our yearly GW early-warning samples with DO-OPT for the four population models in Figure 5; similar distributions for DEC are plotted in Figure 6. We mark all detectable NS-WD mergers with circles in different colours based on their SNRs. Our results seem to suggest that the mergers with higher SNRs tend to have better localization accuracies (i.e., smaller $\Delta\Omega$ and $\Delta D_L/D_L$), which are mainly distributed in the lower left of these plots in Figure 5 and Figure 6. In each plot, the purple histograms show the

¹¹ For cold, slowly rotating WDs, we can see in Figure 2 of [Wolz et al. \(2020\)](#) that Λ_{WD} is of the order of $10^{13}\text{--}10^{21}$. However, in comparison, Λ_{NS} is $\lesssim O(10^3)$ in GW170817 ([Abbott et al. 2017a](#)).

¹² For the merger time uncertainty Δt_c , we find that 90% of the yearly detectable NS-WD mergers (see Table 2) could reach a timing accuracy of $\Delta t_c < O(10^4)$ s level, regardless of the population models and decihertz GW detectors. Even considering the extra exposure time and slew time for EM follow-up facilities, we still regard this as a crude but acceptable treatment to adopt an early-warning time $t_e = 1$ d in this work.

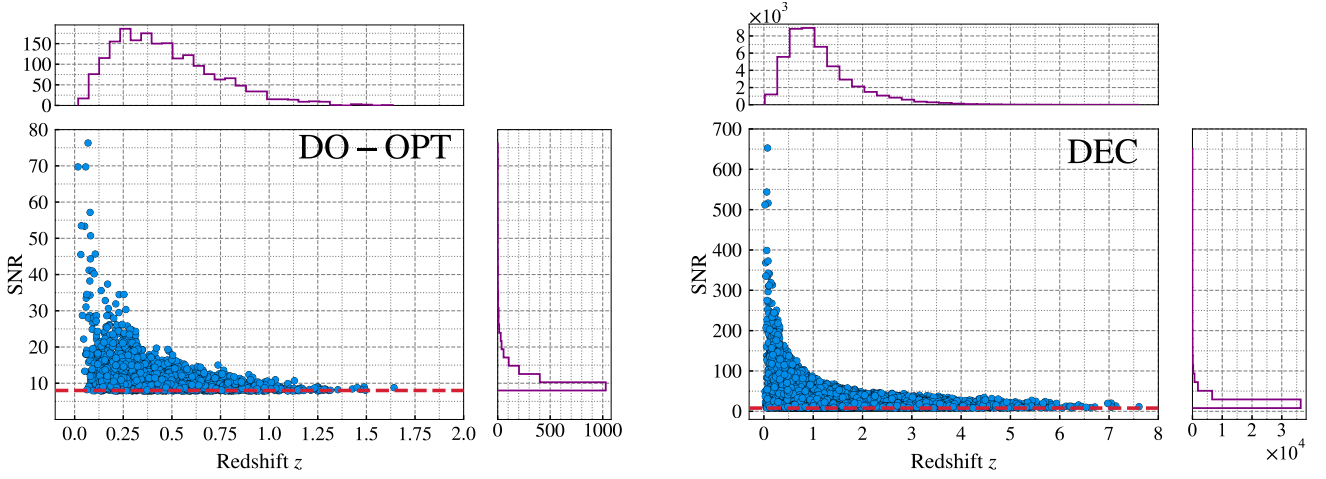


Figure 3. SNR as a function of redshift for yearly detectable NS-WD mergers for DO-OPT (left) and DEC (right). We only show the population Model A as an example. Dashed horizontal red lines correspond to the detection threshold SNR = 8. In each plot, the purple histograms show the redshift and SNR distributions in upper and right panels, respectively.

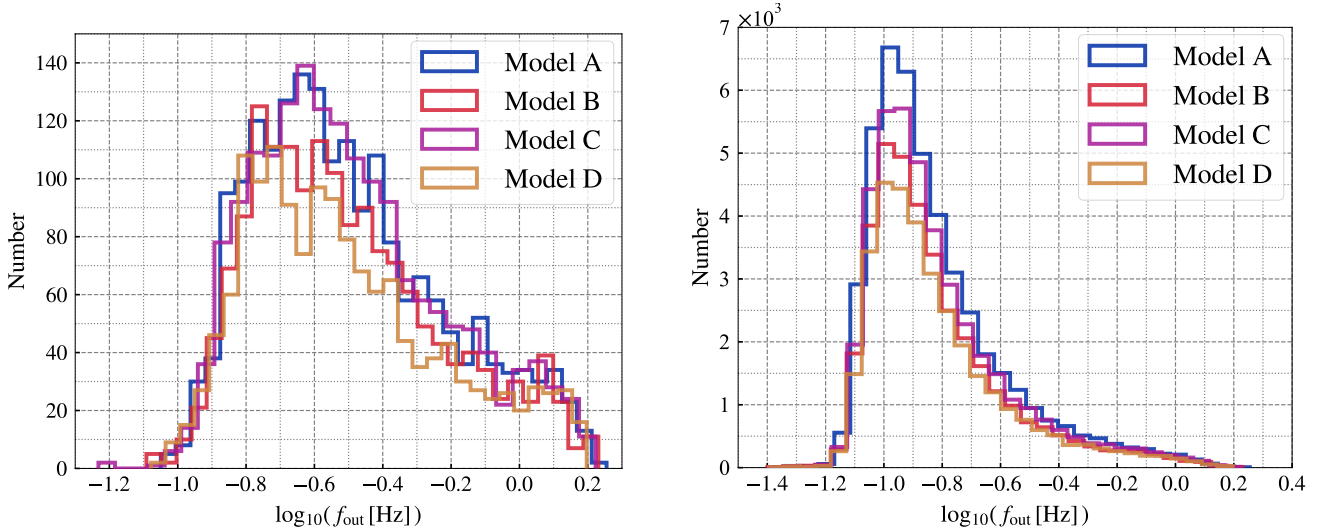


Figure 4. Distributions of f_{out} (defined in Section 3) for detectable NS-WD mergers in DO-OPT (left) and DEC (right). The total numbers of detectable merger events are listed in Table 2. We set the early-warning time to be $t_e = 1$ d. Different colours correspond to different population models.

$\Delta\Omega$ and $\Delta D_L/D_L$ distributions in upper and right panels, respectively. Both Figure 5 and Figure 6 show that the peak of the $\Delta\Omega$ distribution is at $\approx O(0.01)$ deg^2 level, regardless of the population models in our considerations. For the $\Delta D_L/D_L$ distributions, most early-warning samples of DO-OPT are clustered in the range of $0.3 \lesssim \Delta D_L/D_L \lesssim 1$. In comparison, DEC provides more accurate estimations of ΔD_L , given that the peak of the $\Delta D_L/D_L$ distribution is mostly at $\approx O(0.1)$ level.

To go a step further, we are particularly interested in those mergers that would yield the best estimation results of the distance and angular resolution. This is because these events can provide helpful inputs for future multimessenger astronomy with decihertz GW early warnings and EM follow-ups. In view of this, we further define a Golden Sample (denoted as ‘GS’ hereafter) set for our yearly GW early-warning samples with the two criteria that

- (i) $\Delta\Omega < 1 \text{ deg}^2$, and
- (ii) $\Delta D_L/D_L < 0.3$.

Given that many current and planned wide-field optical survey projects have $\text{FoV} \gtrsim 1 \text{ deg}^2$ (e.g., see in Table A2 the summary of the technical information for some optical survey telescopes), we follow the discussions in Kang et al. (2022) to set 1 deg^2 to be the threshold in criterion (i). For criterion (ii), we arbitrarily set 30% to be the selection criterion on $\Delta D_L/D_L$. Note that similar crude treatments in fact are commonly adopted in many studies (e.g., Tamanini & Danielski 2019; Kang et al. 2021). Based on the above analyses, the NS-WD mergers in GS would matter the most to future multimessenger early-warning detections. In Figure 5 and Figure 6 we plot black dashed lines to denote the selection functions corresponding to the criteria (i) and (ii) above. Therefore, the shaded blue regions in Figure 5 and Figure 6 delimit the parameter space of GS.

We list in Table 3 yearly detection numbers of NS-WD mergers in GS for the four population models with DO-OPT and DEC. The percentages in brackets show the ratio to the total number of yearly detectable NS-WD mergers (see Table 2). Combining all the results shown in Table 3, we conclude that DEC performs much better on GS

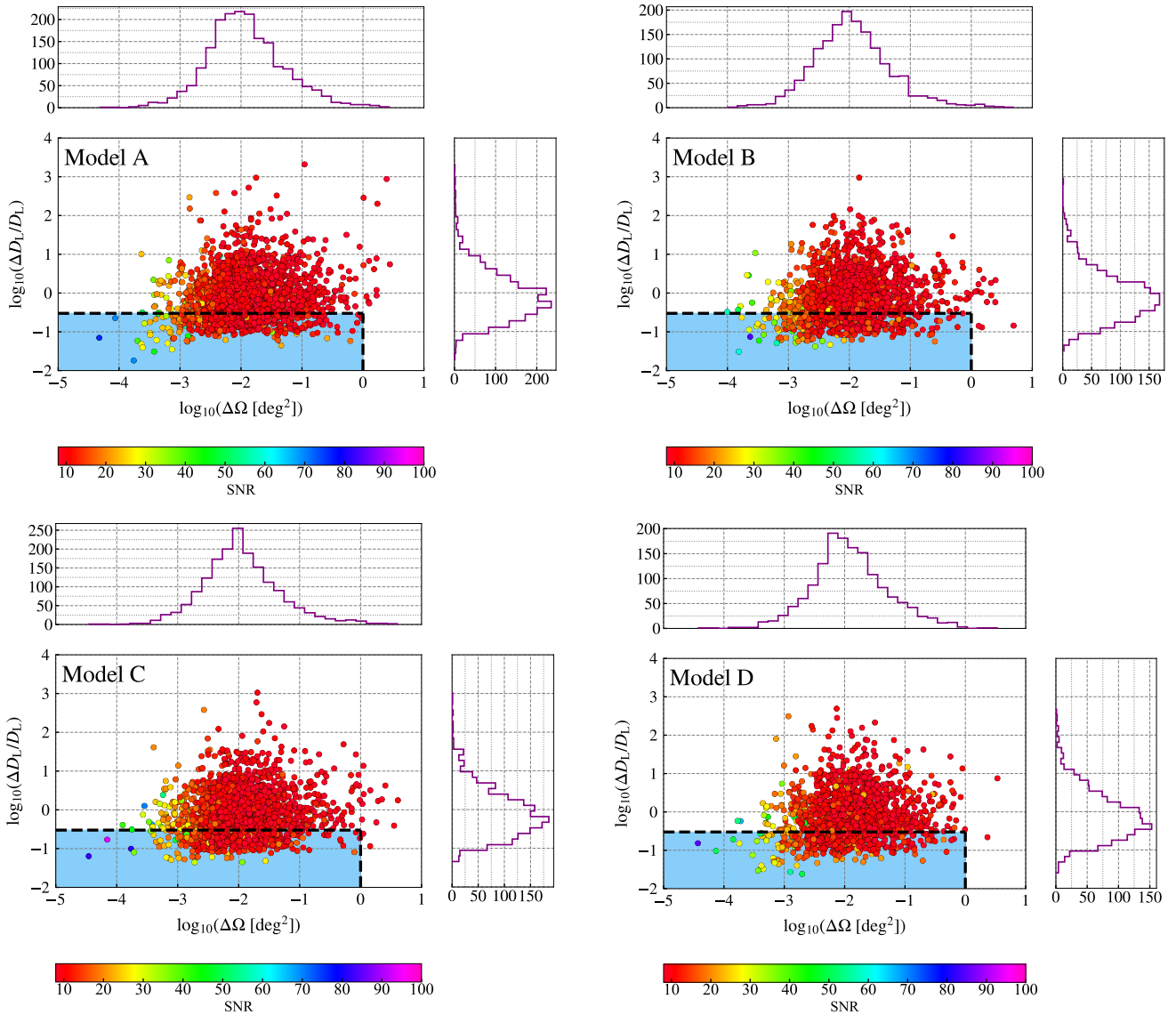


Figure 5. $\Delta D_L/D_L$ versus $\Delta\Omega$ for yearly GW early-warning samples with DO-OPT for different population models. The colour represents the SNR of each merger event. In each plot, the purple histograms show the $\Delta\Omega$ and $\Delta D_L/D_L$ distributions in the upper and right panels, respectively. The black dashed lines denote the dividing lines used to select the GS set in the shaded blue region (see Section 4).

detections as a whole, with its yearly detection number in the range of $\sim (2.1\text{--}2.8) \times 10^4$. In comparison, the GS detection number for DO-OPT is in the range of $\sim (3.8\text{--}4.5) \times 10^2$, which is approximately 50 times fewer than DEC. In particular, we note that the percentage of GS detections with DEC to its total yearly detectable mergers is $\geq 60\%$, while it is much smaller for DO-OPT, with the ratio to be $\leq 25\%$.

Finally, let us move to the potential for future multimessenger early-warning detections of NS-WD mergers. Taking the peculiar IGRB, GRB 211211A, as an example,¹³ the observational facts show that it

is a nearby bright GRB at $z = 0.0763$ (≈ 350 Mpc) with a possible NS-WD merger origin (Rastinejad et al. 2022; Troja et al. 2022; Yang et al. 2022; Mei et al. 2022; Gompertz et al. 2023). Using a set of pseudo-GRBs, Yin et al. (2023) have shown that a GRB 211211A-like event could be detectable up to a maximum redshift $z = 0.52$ (≈ 3000 Mpc). On the other hand, our results suggest that the number of yearly detectable NS-WD mergers with $z \lesssim 0.52$ is in the range of $\sim 990\text{--}1300$ for DO-OPT, and the corresponding percentage to the total number of yearly detectable merger events (see Table 2) is $\sim 65\%$. They are $\sim 5200\text{--}6700$ and $\sim 15\%$ for DEC. Remember that GRBs are highly beamed, so another condition for the detection of a successful GRB event is that its jet should beam towards the Earth.¹⁴

¹³ Recently, there is another extremely bright cb-IGRB, GRB 230307A, at a redshift of $z = 0.065$ (≈ 300 Mpc; Fausnaugh et al. 2023; Levan et al. 2023; Sun et al. 2023; Mereghetti et al. 2023; Gillanders et al. 2023). However, given the different features of the afterglow/kilonova-like emissions and precursor properties from GRB 211211A, most investigation was not in favor of the NS-WD merger origin for GRB 230307A (Wang et al. 2023c; Levan et al.

2023; Dichiaro et al. 2023; Song 2023; Yang et al. 2023a). It is more likely to be a BNS merger.

¹⁴ In the case of a choked jet, the jet energy would be stored in a hot, shocked material, forming a broad cocoon without a spine jet (Zhang 2018). Choked

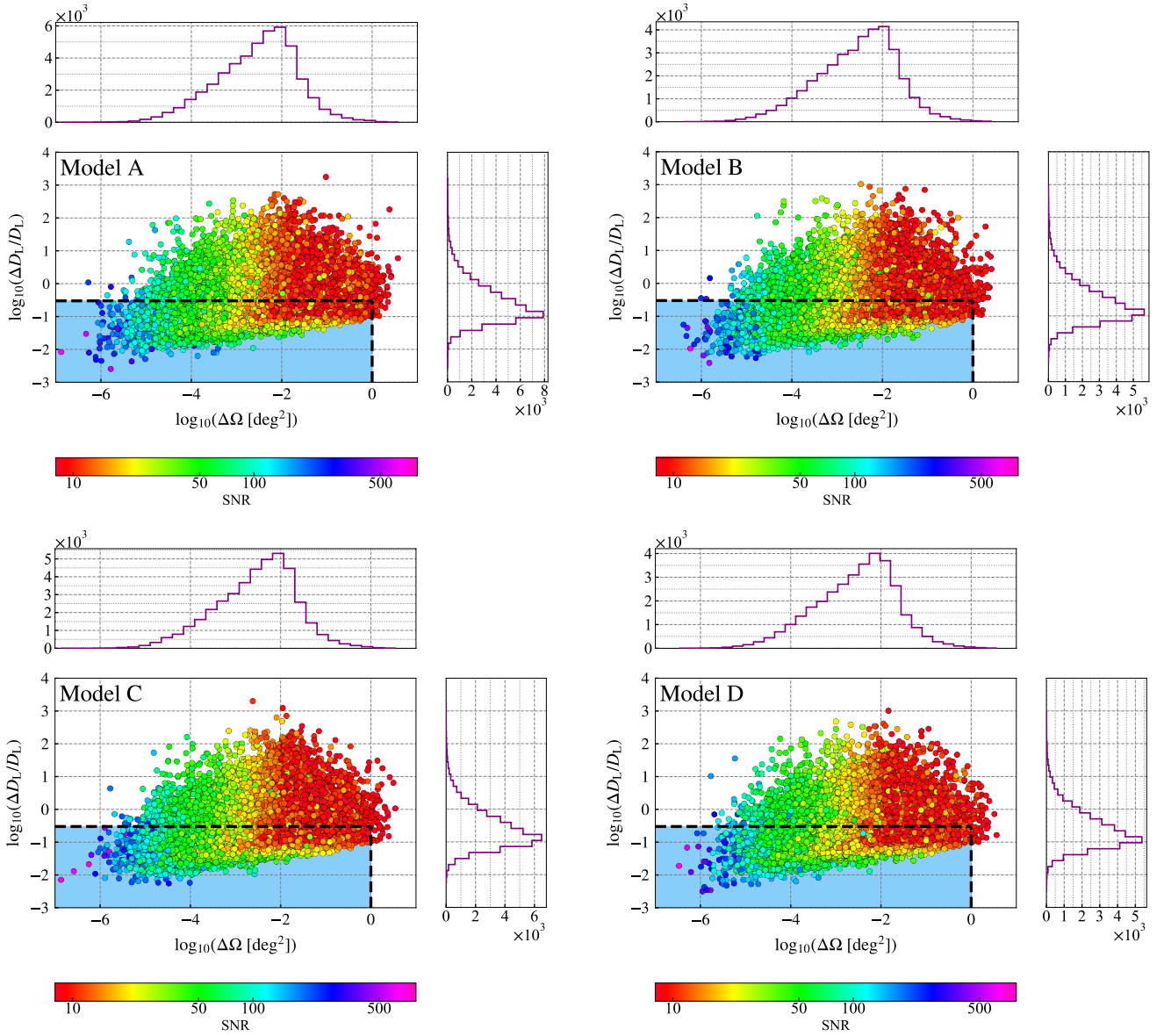


Figure 6. Same as Figure 5, but for DEC. Note that all detectable NS-WD merger events are color-coded by the logarithmic SNRs in each plot.

The beaming factor of a GRB is defined by $f_b \equiv \Delta\Omega_b/4\pi \approx \theta_v^2/2$, where $\Delta\Omega_b$ is the solid angle of a bipolar, conical jet, and θ_v ($\ll 1$) is its half-opening angle. Assuming a typical value of 15° for θ_v , we could obtain $f_b \approx 0.034$. Considering such relativistic beaming effects, there should be a few tens (hundreds) yearly detectable NS-WD mergers that beam towards us for DO-OPT (DEC) within $z \lesssim 0.52$. Given that the properties of NS-WD GRBs are still under debate (see, e.g., King et al. 2007; Zenati et al. 2019; Bobrick et al. 2022; Morán-Fraile et al. 2024; Ablimit & Soker 2024), we point out here that if there are $\geq 1\%$ of NS-WD mergers with $z \lesssim 0.52$ that can successfully produce GRB 211211A-like signals, the possibility of multimessenger early-warning detections indeed exists during a 4-yr mission time for decihertz GW detectors. This also means that future

jets could have larger viewing angles and be even more abundant than those that successfully break out. This topic deserves more detailed analyses.

multimessenger early-warning detections could help people constrain the fraction of NS-WD systems that are capable of producing GRBs.

Besides the peculiar GRB signal, optical/infrared kilonova emissions associated with GRB 211211A were also observed. Many recent studies have proposed various kilonova models and suggest that the peak AB absolute magnitude of GRB 211211A-like kilonovae should be ≈ -17 in g , r , and i bands (Yang et al. 2022; Barnes & Metzger 2023; Kunert et al. 2024; Zhong et al. 2023). Based on the above finding, if we set $z = 0.52$ as the redshift upper limit for detections of GRB 211211A-like events, the limiting magnitude m^* for wide-field optical survey projects should satisfy $m^* \gtrsim 25$ to ensure the kilonova detections. From Table A2 we find that LSST and CSST meet the above requirements well. Therefore, more cooperative observations with different optical surveys and decihertz GW detectors would be very promising in the future. Given that the true nature of GRB 211211A-like events remains unknown, we emphasize that the multimessenger observations with GW early warnings and the above multiband EM follow-ups would shed light on the origin of

Table 3. Yearly detection numbers and percentages (in brackets) of NS-WD mergers in the GS for different population models with DO-OPT and DEC. Note that the percentages in brackets show the ratio to the total number of yearly detectable NS-WD mergers (see Table 2).

| GW Detector | Population Model | | | |
|-------------|--------------------|--------------------|--------------------|--------------------|
| | A | B | C | D |
| DO-OPT | 451 (23.55 %) | 396 (24.19 %) | 428 (24.85 %) | 378 (25.39 %) |
| DEC | 28229 (61.30 %) | 22320 (61.77 %) | 25301 (61.30 %) | 20677 (62.07 %) |

such peculiar IGRBs. Note that even for the NS-WD merger scenario, the properties of their EM follow-up transients could vary widely, depending on the component masses, the magnetic field strength and configuration, specific afterglow and kilonova models, *etc.*¹⁵ We leave the impacts of those uncertainties on the realistic multimessenger observations for future studies.

5 CONCLUSION

In this work, we follow Liu et al. (2022b) to discuss GW detections and early-warning predictions of NS-WD mergers with two spaceborne decihertz GW detectors, DO-OPT and DEC. Based on different SFR and DTD models, we use the method of convolution with a series of Monte Carlo simulations to obtain four NS-WD merger population models. For all NS-WD mergers with the merger time $1 \text{ yr} \leq t_{c0} \leq 2 \text{ yr}$, we set the early-warning time to $t_e = 1 \text{ d}$ and SNR threshold to 8 to perform GW detection strategy. Based on the NS-WD merger populations, we not only give quick assessments of GW detection rates with the two decihertz GW detectors, but also report systematic analyses on the characteristics of GW-detectable merger events using the FIM. We find that DEC has better performance than DO-OPT as a whole, especially for high- z events. The yearly GW detection number for DEC is in the range of $\sim (3.3\text{--}4.6) \times 10^4$, while it is only $\sim (1.5\text{--}1.9) \times 10^3$ for DO-OPT, approximately 20 times fewer. Taking the population Model A as an example, DO-OPT can detect early-warning sources up to $z \leq 1.7$, while DEC could reach $z \leq 7.6$. Moreover, detectable NS-WD mergers are clustered at $z \approx 0.8$ for DEC. In comparison, due to the limited detection abilities, most detectable NS-WD mergers are clustered around $z \approx 0.25$ for DO-OPT. Similarly, for the maximum SNR, we show that DEC reaches $\text{SNR} \approx 650$, while DO-OPT reaches $\text{SNR} \approx 75$.

Differently from BNS mergers or NS-BH mergers, we note that GW early-warning detections of NS-WD mergers are essentially to offer alerts on the RLOF time, especially considering that there is no well-modeled GW waveform for NS-WD systems during the runaway mass-transfer phase. In view of this, for the FIM in the frequency domain, the integration upper limit f_{out} should be related to the GW cutoff frequency at the critical RLOF separation. We plot the distributions of f_{out} for detectable NS-WD mergers observed by DO-OPT and DEC. The majority of total detectable NS-WD mergers for DEC cluster at $f_{\text{out}} \approx 0.1 \text{ Hz}$, while in comparison, the peak of f_{out} distribution for DO-OPT is a little higher in a wider range (0.16–0.25 Hz).

¹⁵ For example, Yang et al. (2022) pointed out that a massive WD component near the Chandrasekhar mass limit should be involved to trigger the accretion-induced collapse of the WD during the GRB 211211A event.

These could be explained by the cosmological redshift effect, given that DEC will detect more high- z events.

As for the estimations of the accuracy of distance and angular resolution, we compare $\Delta D_L/D_L$ - $\Delta\Omega$ distributions of yearly GW early-warning samples for DO-OPT and DEC with different population models. Our results show that the peak of the $\Delta\Omega$ distribution is expected to be at $\approx O(0.01) \text{ deg}^2$ level, regardless of the changes in decihertz GW detectors and population models. For the $\Delta D_L/D_L$ distributions, most early-warning samples of DO-OPT are clustered in the range of $0.3 \lesssim \Delta D_L/D_L \lesssim 1$, while in comparison, DEC can provide more accurate estimations of ΔD_L , given that the peak of the $\Delta D_L/D_L$ distribution is at $\approx O(0.1)$ level. Furthermore, for those mergers that would yield the best estimation results of the distance and angular resolution, we define them as a GS. We present the yearly detection numbers of NS-WD mergers in GS for different population models with DO-OPT and DEC. We conclude that DEC performs much better on GS detections as a whole, with its yearly detection number in the range of $\sim (2.1\text{--}2.8) \times 10^4$, while it is $\sim (3.8\text{--}4.5) \times 10^2$ for DO-OPT, approximately 50 times fewer than DEC. The percentage of GS detections with DEC to its total yearly detectable NS-WD mergers could achieve $\geq 60\%$, while it is much smaller for DO-OPT with the ratio to be $\leq 25\%$.

Finally, taking the recent peculiar IGRB, GRB 211211A, as an example, we further discuss the potential for future multimessenger early-warning detections of NS-WD mergers. With a sufficient early-warning time (e.g., $t_e = 1 \text{ d}$) and the localization accuracies, we suggest that the GW early-warning detection will allow future EM telescopes to prepare well in advance for the possible follow-up transients after some special NS-WD mergers. Given that the nature of cb-IGRBs remains an open question, the multimessenger observations with the GW early warnings and the multiband EM follow-ups are expected to shed new light on their properties. For example, compared with BNS and NS-BH scenarios, no inspiral GW signals of NS-WD mergers are expected to enter the ground-based detectors following decihertz GW early warnings. The EM follow-up transients with different origins may also vary widely. In view of this, our results can provide meaningful references and helpful inputs for upcoming EM follow-up projects.

There are, of course, many ways in which this study can be extended. At the end of Section 3, we have emphasized that precise GW-waveform constructions should take into account the effects of mass transfer and dynamical tides for WDs, especially in the late inspiral stages of NS-WD mergers. Also, our results leave out the consideration of the confusion noise (Christensen 2019), which depends strongly on the specific population model, the sensitivity of the detector, and its operation time, *etc.*¹⁶ We also leave out the dedi-

¹⁶ It has been shown that the confusion noise from DCOs could be sub-

cated analyses of overlapping signals which may affect the parameter estimation (see e.g., Wang et al. 2023a), but we expect our result unlikely to change significantly even when overlapping signals are considered. Moreover, the realistic multimessenger searching strategy, including the communication between GW detectors and EM telescopes, should be considered. On the other hand, even if there are no observable EM transients after NS-WD mergers, we suggest that the GW-detectable NS-WD populations in GS could still be of great use for the dark-siren cosmology (see, e.g., Schutz 1986; Fishbach et al. 2019; Soares-Santos et al. 2019; Zhu et al. 2022a,b; Liu et al. 2022a; Yang et al. 2023b; Seymour et al. 2023). We hope that more studies can be carried out in the future.

ACKNOWLEDGEMENTS

We would like to thank the anonymous referee for helpful and valuable comments and suggestions. This work was supported by the Beijing Municipal Natural Science Foundation (1242018), the National Natural Science Foundation of China (11975027, 11991053, 11721303, U2038105, U1831135, 12121003, 12103065), the National SKA Program of China (2020SKA0120300, 2022SKA0130102), the National Key Research and Development Programs of China (2022YFF0711404), the science research grants from the China Manned Space Project with No. CMS-CSST-2021-B11, the Max Planck Partner Group Program funded by the Max Planck Society, the Fundamental Research Funds for the Central Universities, the Program for Innovative Talents and Entrepreneur in Jiangsu, and the High-Performance Computing Platform of Peking University. C.L. was supported by the China Scholarship Council (CSC).

DATA AVAILABILITY

The data underlying this paper will be shared on a reasonable request to the corresponding authors.

REFERENCES

Abbott B. P., et al., 2017a, *Phys. Rev. Lett.*, 119, 161101
 Abbott B. P., et al., 2017b, *ApJ*, 848, L13
 Abbott B. P., et al., 2017c, *ApJ*, 850, L39
 Abbott B. P., et al., 2018a, *Living Rev. Relativ.*, 21, 3
 Abbott B. P., et al., 2018b, *Phys. Rev. Lett.*, 121, 161101
 Abbott B. P., et al., 2019, *Phys. Rev. Lett.*, 123, 011102
 Abell P. A., et al., 2009, preprint, p. (arXiv:0912.0201)
 Ablimit I., Soker N., 2024, *MNRAS*, 527, 205
 Aghanim N., et al., 2020, *A&A*, 641, A6
 Amaro-Seoane P., et al., 2023, *Living Rev. Relativ.*, 26, 2
 Arun K. G., et al., 2022, *Living Rev. Relativ.*, 25, 4
 Banerjee B., et al., 2023, *A&A*, 678, A126
 Barack L., Cutler C., 2004, *Phys. Rev. D*, 69, 082005
 Barnes J., Metzger B. D., 2023, *ApJ*, 947, 55
 Baum S., Bogorad Z., Graham P. W., 2023, preprint, p. (arXiv:2309.07952)
 Bayle J.-B., Bonga B., Caprini C., Doneva D., Muratore M., Petiteau A., Rossi E., Shao L., 2022, *Nature Astron.*, 6, 1334
 Becker W., Prinz T., Winkler P. F., Petre R., 2012, *ApJ*, 755, 141
 Bellm E. C., et al., 2019, *PASP*, 131, 018002

tracted out by an iteration scheme and a global fit (Cutler & Harms 2006). More related discussions on the impact of confusion noise for decihertz GW detectors can be found in Liu et al. (2022b).

Bobrick A., Davies M. B., Church R. P., 2017, *MNRAS*, 467, 3556
 Bobrick A., Zenati Y., Perets H. B., Davies M. B., Church R., 2022, *MNRAS*, 510, 3758
 Branchesi M., et al., 2023, *J. Cosmology Astropart. Phys.*, 07, 068
 Chatterjee S., et al., 2005, *ApJ*, 630, L61
 Chattopadhyay T., Misra R., Chattopadhyay A. K., Naskar M., 2007, *ApJ*, 667, 1017
 Christensen N., 2019, *Rept. Prog. Phys.*, 82, 016903
 Cordes J. M., Romani R. W., Lundgren S. C., 1993, *Nature*, 362, 133
 Coulter D. A., et al., 2017, *Science*, 358, 1556
 Cutler C., 1998, *Phys. Rev. D*, 57, 7089
 Cutler C., Flanagan E. E., 1994, *Phys. Rev. D*, 49, 2658
 Cutler C., Harms J., 2006, *Phys. Rev. D*, 73, 042001
 Dichiaro S., Tsang D., Troja E., Neill D., Norris J. P., Yang Y. H., 2023, *ApJ*, 954, L29
 Eggleton P. P., 1983, *ApJ*, 268, 368
 Eichler D., Livio M., Piran T., Schramm D. N., 1989, *Nature*, 340, 126
 Evans P. A., et al., 2017, *Science*, 358, 1565
 Fausnaugh M. M., et al., 2023, *Res. Notes AAS*, 7, 56
 Favata M., 2014, *Phys. Rev. Lett.*, 112, 101101
 Fernández R., Margalit B., Metzger B. D., 2019, *MNRAS*, 488, 259
 Finn L. S., 1992, *Phys. Rev. D*, 46, 5236
 Fishbach M., et al., 2019, *ApJ*, 871, L13
 Flanagan E. E., Hinderer T., 2008, *Phys. Rev. D*, 77, 021502
 Gillanders J. H., Sim S. A., Smartt S. J., 2020, *MNRAS*, 497, 246
 Gillanders J. H., et al., 2023, preprint, p. (arXiv:2308.00633)
 Goldstein A., et al., 2017, *ApJ*, 848, L14
 Gompertz B. P., et al., 2023, *Nat. Astron.*, 7, 67
 Gong Y., et al., 2019, *ApJ*, 883, 203
 Gunn J. E., Ostriker J. P., 1970, *ApJ*, 160, 979
 Harms J., et al., 2021, *ApJ*, 910, 1
 Hinderer T., 2008, *ApJ*, 677, 1216
 Hobbs G., Lorimer D. R., Lyne A. G., Kramer M., 2005, *MNRAS*, 360, 974
 Ivanova N., et al., 2013, *A&A Rev.*, 21, 59
 Ivezić v., et al., 2019, *ApJ*, 873, 111
 Jani K., Loeb A., 2021, *J. Cosmology Astropart. Phys.*, 06, 044
 Kalogera V., Narayan R., Spergel D. N., Taylor J. H., 2001, *ApJ*, 556, 340
 Kaltenborn M. A. R., Fryer C. L., Wollaeger R. T., Belczynski K., Even W., Kouveliotou C., 2023, *ApJ*, 956, 71
 Kang Y., Liu C., Shao L., 2021, *AJ*, 162, 247
 Kang Y., Liu C., Shao L., 2022, *MNRAS*, 515, 739
 Kang Y., Liu C., Zhu J., Shao L., 2023, *Sci. China Phys. Mech. Astron.*, 53, 100014
 Kawamura S., et al., 2011, *Class. Quantum Gravity*, 28, 094011
 Kawamura S., et al., 2021, *Prog. Theor. Exp. Phys.*, 2021, 05A105
 Khokhriakova A. D., Popov S. B., 2019, *J. High Energy Astrophys.*, 24, 1
 Kilpatrick C. D., et al., 2017, *Science*, 358, 1583
 Kim C.-L., Kalogera V., Lorimer D. R., White T., 2004, *ApJ*, 616, 1109
 King A., Olsson E., Davies M. B., 2007, *MNRAS*, 374, L34
 Kopparapu R. K., Hanna C., Kalogera V., O’Shaughnessy R., González G., Brady P. R., Fairhurst S., 2008, *ApJ*, 675, 1459
 Kremer K., Breivik K., Larson S. L., Kalogera V., 2017, *ApJ*, 846, 95
 Kunert N., et al., 2024, *MNRAS*, 527, 3900
 Kuns K. A., Yu H., Chen Y., Adhikari R. X., 2020, *Phys. Rev. D*, 102, 043001
 Kyutoku K., Okawa H., Shibata M., Taniguchi K., 2011, *Phys. Rev. D*, 84, 064018
 Lai J. F. D., 2012, *MNRAS*, 421, 426
 Lamberts A., et al., 2018, *MNRAS*, 480, 2704
 Lau S. Y., Yagi K., Arras P., 2022, *Phys. Rev. D*, 106, 103038
 Leván A., et al., 2023, preprint, p. (arXiv:2307.02098)
 Li L.-X., Paczynski B., 1998, *ApJ*, 507, L59
 Li J., et al., 2023, *Sci. China Phys. Mech. Astron.*, 66, 109513
 Liu C., Shao L., 2022, *ApJ*, 926, 158
 Liu C., Shao L., Zhao J., Gao Y., 2020, *MNRAS*, 496, 182
 Liu M., Liu C., Hu Y.-M., Shao L., Kang Y., 2022a, *Phys. Dark Univ.*, 38, 101136
 Liu C., Kang Y., Shao L., 2022b, *ApJ*, 934, 84
 Livio M., Mazzali P., 2018, *Phys. Rept.*, 736, 1

- Lyne A. G., Lorimer D. R., 1994, *Nature*, 369, 127
- Madau P., Dickinson M., 2014, *ARA&A*, 52, 415
- Maggiore M., 2008, *Gravitational Waves. Vol. 1: Theory and Experiments.* Oxford Univ. Press, Oxford, Oxford Master Series in Physics
- Maggiore M., et al., 2020, *J. Cosmology Astropart. Phys.*, 03, 050
- Margalit B., Metzger B. D., 2016, *MNRAS*, 461, 1154
- Margalit B., Metzger B. D., 2017, *MNRAS*, 465, 2790
- Masci F. J., et al., 2019, *PASP*, 131, 018003
- McNeill L. O., Mardling R. A., Müller B., 2020, *MNRAS*, 491, 3000
- Mei A., et al., 2022, *Nature*, 612, 236
- Mereghetti S., Rigoselli M., Salvaterra R., Tiengo A., Pacholski D. P., 2023, *ApJ*, 956, 97
- Metzger B. D., 2012, *MNRAS*, 419, 827
- Morán-Fraile J., Röpke F. K., Pakmor R., Aloy M. A., Ohlmann S. T., Schneider F. R. N., Leidi G., Lioutas G., 2024, *Astron. & Astrophys.*, 681, A41
- Narayan R., Paczynski B., Piran T., 1992, *ApJ*, 395, L83
- Nauenberg M., 1972, *ApJ*, 175, 417
- Nelemans G., Yungelson L. R., Portegies Zwart S. F., Verbunt F., 2001a, *A&A*, 365, 491
- Nelemans G., Yungelson L. R., Portegies Zwart S. F., 2001b, *A&A*, 375, 890
- O’Shaughnessy R., Kim C., 2010, *ApJ*, 715, 230
- Paczynski B., 1986, *ApJ*, 308, L43
- Paschalidis V., MacLeod M., Baumgarte T. W., Shapiro S. L., 2009, *Phys. Rev. D*, 80, 024006
- Paschalidis V., Liu Y. T., Etienne Z., Shapiro S. L., 2011, *Phys. Rev. D*, 84, 104032
- Pian E., et al., 2017, *Nature*, 551, 67
- Rastinejad J. C., et al., 2022, *Nature*, 612, 223
- Reitze D., et al., 2019, *Bull. Am. Astron. Soc.*, 51, 35
- Ronchini S., et al., 2022, *A&A*, 665, A97
- Ruiter A. J., 2020, *Int. Astron. Union Symp.*, 357, 1
- Sathyaprakash B., et al., 2019, *BAAAS*, 51, 251
- Savchenko V., et al., 2017, *ApJ*, 848, L15
- Schutz B. F., 1986, *Nature*, 323, 310
- Sedda M. A., et al., 2020, *Class. Quantum Gravity*, 37, 215011
- Sedda M. A., et al., 2021, *Exper. Astron.*, 51, 1427
- Seymour B. C., Yu H., Chen Y., 2023, *Phys. Rev. D*, 108, 044038
- Shao L., 2023, *Sci. China Phys. Mech. Astron.*, 66, 119531
- Shao L., Sennett N., Buonanno A., Kramer M., Wex N., 2017, *Phys. Rev. X*, 7, 041025
- Shi D. D., Zheng X. Z., Zhao H. B., Lou Z., Wang H. R., Qian Y., Liu W., Yao D. Z., 2018, *Acta Astron. Sin.*, 59, 22
- Shibata M., Taniguchi K., 2011, *Living Rev. Relativ.*, 14, 6
- Soares-Santos M., et al., 2019, *ApJ*, 876, L7
- Soker N., 2018, *SCPMA*, 61, 049502
- Song X.-Y., 2023, *ApJ*, 958, 133
- Sun H., Zhang B., Li Z., 2015, *ApJ*, 812, 33
- Sun H., et al., 2023, preprint, p. (arXiv:2307.05689)
- Tamanini N., Danielski C., 2019, *Nat. Astron.*, 3, 858
- Tauris T. M., 2018, *Phys. Rev. Lett.*, 121, 131105
- Toonen S., Perets H. B., Igoshev A. P., Michaely E., Zenati Y., 2018, *A&A*, 619, A53
- Troja E., et al., 2022, *Nature*, 612, 228
- Verbunt F., Rappaport S., 1988, *ApJ*, 332, 193
- Verbunt F., Igoshev A., Cator E., 2017, *A&A*, 608, A57
- Virgili F. J., Zhang B., O’Brien P., Troja E., 2011, *ApJ*, 727, 109
- Wanderman D., Piran T., 2015, *MNRAS*, 448, 3026
- Wang B., 2018, *Res. Astron. Astrophys.*, 18, 049
- Wang Z., Liu C., Zhao J., Shao L., 2022, *Astrophys. J.*, 932, 102
- Wang Z., Liang D., Zhao J., Liu C., Shao L., 2023a, *arXiv e-prints*, p. arXiv:2304.06734
- Wang T., et al., 2023b, *Sci. China Phys. Mech. Astron.*, 66, 109512
- Wang Y., Xia Z.-Q., Zheng T.-C., Ren J., Fan Y.-Z., 2023c, *ApJ*, 953, L8
- Waxman E., Ofek E. O., Kushnir D., 2022, preprint, p. (arXiv:2206.10710)
- Wolz A., Yagi K., Anderson N., Taylor A. J., 2020, *MNRAS*, 500, L52
- Yang J., et al., 2022, *Nature*, 612, 232
- Yang Y.-H., et al., 2023a, preprint, p. (arXiv:2308.00638)
- Yang T., Cai R.-G., Cao Z., Lee H. M., 2023b, *Phys. Rev. D*, 107, 043539
- Yin Y.-H. I., Zhang B.-B., Sun H., Yang J., Kang Y., Shao L., Yang Y.-H., Zhang B., 2023, *ApJ*, 954, L17
- Yuan X., et al., 2020, *Proc. SPIE*, 11445, 114457M
- Yuksel H., Kistler M. D., Beacom J. F., Hopkins A. M., 2008, *ApJ*, 683, L5
- Zenati Y., Perets H. B., Toonen S., 2019, *MNRAS*, 486, 1805
- Zhang B., 2018, *The Physics of Gamma-Ray Bursts.* Cambridge University Press, Cambridge
- Zhang B. B., et al., 2018, *Nat. Commun.*, 9, 447
- Zhao J., Shao L., Gao Y., Liu C., Cao Z., Ma B.-Q., 2021a, *Phys. Rev. D*, 104, 084008
- Zhao Z. Y., Zhang G. Q., Wang Y. Y., Tu Z. L., Wang F. Y., 2021b, *ApJ*, 907, 111
- Zhong S.-Q., Li L., Dai Z.-G., 2023, *ApJ*, 947, L21
- Zhu J.-P., et al., 2021, *ApJ*, 917, 24
- Zhu L.-G., Hu Y.-M., Wang H.-T., Zhang J.-d., Li X.-D., Hendry M., Mei J., 2022a, *Phys. Rev. Res.*, 4, 013247
- Zhu L.-G., et al., 2022b, *Sci. China Phys. Mech. Astron.*, 65, 259811
- Zhu J.-P., Wang X. I., Sun H., Yang Y.-P., Li Z., Hu R.-C., Qin Y., Wu S., 2022c, *ApJ*, 936, L10
- Zhu J.-P., et al., 2023, *ApJ*, 942, 88

APPENDIX A: THE REDSHIFT DISTRIBUTION FACTOR

As mentioned in Section 2, when we ignore the possible redshift evolution of intrinsic system parameters for NS-WD mergers, the redshift-dependent merger event rate density $\dot{\rho}(z)$ is,

$$\dot{\rho}(z) = \dot{\rho}_0 f(z), \quad (\text{A1})$$

where z is the redshift, $\dot{\rho}_0$ is the local NS-WD event rate density, and $f(z)$ is the dimensionless redshift distribution factor. On the other hand, $\dot{\rho}(z)$ can also connect to the cosmological SFR density $\dot{\rho}_*(z)$ by accounting for the probability density function of delay time $P(\tau)$ of NS-WD mergers via

$$\begin{aligned} \dot{\rho}(z) &\propto \int_{\tau_{\min}}^{\tau_{\max}} \dot{\rho}_* [z'(\tau)] P(\tau) d\tau \\ &\propto \int_{z'_{\min}}^{z'_{\max}} \dot{\rho}_* (z') P [\tau (z')] \left[-\frac{dt(z')}{dz'} \right] dz', \end{aligned} \quad (\text{A2})$$

where $\tau = t(z) - t(z')$ is the delay time¹⁷ and $t(z')$ is the time when the binaries are formed with two zero-age main sequence stars, $t(z)$ is the merger time for such binaries, and τ_{\min} and τ_{\max} are the minimum and maximum delay times, respectively.

With Equations (A1) and (A2), we can obtain $f(z)$ by normalizing it to unity in the local Universe (i.e., $z = 0$). Note that here t is the age of the Universe and we have,

$$\frac{dt(z)}{dz} = -\frac{1}{H_0(1+z)\sqrt{\Omega_\Lambda + (1+z)^3\Omega_m}}. \quad (\text{A3})$$

Therefore, for NS-WD mergers at a fixed z , we can calculate the corresponding z'_{\min} by the definition of τ_{\min} and Equation (A3). Based on the population-synthesis results presented in Toonen et al. (2018), we set $\tau_{\min} = 0.1$ Gyr in our calculations. Following Khokhriakova & Popov (2019), we also set the upper integration redshift limit z'_{\max} to be 11.247 (corresponding to the time when the age of our Universe was 400 Myr) when the intensive star formation began.

For the SFR density $\dot{\rho}_*(z)$, we consider two kinds of analytical models from Yuksel et al. (2008) and Madau & Dickinson (2014)

¹⁷ As defined in Section 3.2.1 of Toonen et al. (2018), the delay time is the evolutionary time between the merger and formation of the binary with two zero-age main sequence stars.

Table A1. The best-fit α_t values derived from different DTDs shown in Section 3.2.1 of [Toonen et al. \(2018\)](#) by Equation (A6). We consider four combinations of two CE evolution models (model ‘ $\alpha\alpha$ ’ and model ‘ $\gamma\alpha$ ’) and two SN-kick velocity distributions (abbreviated as ‘H’ and ‘V’). More details about these models are given in Appendix A.

| Model | α_t |
|-------------------|------------|
| $\alpha\alpha$ -H | -1.12 |
| $\alpha\alpha$ -V | -0.98 |
| $\gamma\alpha$ -H | -1.11 |
| $\gamma\alpha$ -V | -0.95 |

(abbreviated as ‘Y08’ and ‘MD14’, respectively) in our work. They read,

$$\dot{\rho}_*^{\text{Y08}}(z) \propto \left[(1+z)^{3.4\eta} + \left(\frac{1+z}{5000} \right)^{-0.3\eta} + \left(\frac{1+z}{9} \right)^{-3.5\eta} \right]^{1/\eta}, \quad (\text{A4})$$

$$\dot{\rho}_*^{\text{MD14}}(z) \propto \frac{(1+z)^{2.7}}{1 + [(1+z)/2.9]^{5.6}}. \quad (\text{A5})$$

Note that $\eta = -10$ is adopted in Equation (A4).

As for the probability density function of delay time $P(\tau)$, many studies have assumed some empirical forms and derived the best-fit parameters with simulated data. Such a treatment has been widely applied to other DCO systems (e.g., BNS and NS-BH systems; [Virgili et al. 2011](#); [Wanderman & Piran 2015](#); [Sun et al. 2015](#); [Zhu et al. 2021](#)). Therefore, for simplicity, we assume a power-law dependence for the DTD of NS-WD mergers,

$$P(\tau) \propto \tau^{-\alpha_t}, \quad (\text{A6})$$

where α_t is a phenomenological parameter. Considering different common-envelope (CE) evolutions¹⁸ and different NS natal-kick¹⁹ distributions, [Toonen et al. \(2018\)](#) have recently presented different DTDs of NS-WD mergers. Here, we fit four kinds of DTDs taken from [Toonen et al. \(2018\)](#)—abbreviated as ‘ $\alpha\alpha$ -H’, ‘ $\alpha\alpha$ -V’, ‘ $\gamma\alpha$ -H’, and ‘ $\gamma\alpha$ -V’—by Equation (A6) and derive the best-fit α_t values, which are listed in Table A1. Note that ‘ α ’ and ‘ γ ’ are commonly used to denote different treatments for the CE phase where the ‘ α ’-formalism is based on the energy conservation while the ‘ γ ’-formalism is based on the balance of angular momentum instead of the energy ([Ivanova et al. 2013](#)). More specifically, following [Toonen et al. \(2018\)](#), we use ‘ $\alpha\alpha$ ’ and ‘ $\gamma\alpha$ ’ to denote two kinds of CE evolutionary models for NS-WD mergers where the ‘ α ’-prescription is used to determine the outcome of every CE in model ‘ $\alpha\alpha$ ’. In model ‘ $\gamma\alpha$ ’, the ‘ γ ’-prescription is introduced to describe the first CE phase, while the ‘ α ’-prescription is applied in the second CE phase. For SN-kick velocity distributions, we adopt two kinds of models from [Hobbs et al. \(2005\)](#) and [Verbunt et al. \(2017\)](#), respectively (abbreviated as ‘H’ and ‘V’ when combined with model ‘ $\alpha\alpha$ ’ and model ‘ $\gamma\alpha$ ’). The

former (i.e., ‘H’) is a Maxwellian distribution with a one-dimensional root mean square of $\sigma_H = 265 \text{ km s}^{-1}$, while the latter (i.e., ‘V’) includes two Maxwellian components with $\sigma_V^1 = 75 \text{ km s}^{-1}$ and $\sigma_V^2 = 316 \text{ km s}^{-1}$ from a direct comparison of pulsar parallaxes and proper motions. More detailed descriptions of the above DTDs can be found in [Toonen et al. \(2018\)](#).

Based on the above SFR and DTD models, we follow [Zhu et al. \(2021\)](#) to use the method of convolution by Equation (A2) and obtain the dimensionless redshift distribution factor $f(z)$, which are shown in Figure A1. Given a specific DTD model, Figure A1 shows that $f(z)$ has a dramatic dependence on the SFR model in the relatively lower redshift regime ($z \lesssim 4.5$), while in the high- z regime ($z > 4.5$), there is little difference between the Y08 SFR model and the MD14 model. On the other hand, when we adopt the same SFR model, both Table A1 and Figure A1 suggest that different CE evolution models will not influence $f(z)$ significantly, while $f(z)$ can be indeed influenced by the choice of the SN-kick velocity distribution. For this reason, we decide to report detailed analyses only between the model $\gamma\alpha$ -H and the model $\gamma\alpha$ -V in the main text for more in-depth comparisons.

APPENDIX B: INFORMATION FOR OPTICAL SURVEYS

Technical parameters for five current and planned optical time-domain surveys are listed in Table A2, which are: the Zwicky Transient Facility (ZTF; [Masci et al. 2019](#); [Bellm et al. 2019](#)); the Large Synoptic Survey Telescope (LSST, newly named as the Vera Rubin Observatory; [Abell et al. 2009](#); [Ivezić et al. 2019](#)); the Wide Field Survey Telescope (WFST; [Shi et al. 2018](#); [Wang et al. 2023b](#)); the Multi-channel Photometric Survey Telescope (Mephisto; [Yuan et al. 2020](#)); and the Chinese Space Station Telescope (CSST; [Gong et al. 2019](#)). Given the search limiting magnitude m^* , one can obtain the effective limiting flux F_ν^* for each survey telescope by $F_\nu^* \approx 3631 \text{ Jy} \times 10^{-m^*/2.5}$. Note that Table A2 only lists m^* values with the three most common bands (g, r, i), assuming a 300-s exposure time for each survey.

Recently, [Kang et al. \(2022\)](#) have investigated the prospects of multimessenger early-warning detections for BNS mergers, with the help of early warnings from different decihertz GW observatories and optical survey missions. We leave similar analyses on NS-WD mergers for future studies.

This paper has been typeset from a $\text{\TeX}/\text{\LaTeX}$ file prepared by the author.

¹⁸ As a mass-loss phase in the formation of DCO systems, CE evolution can lead to a severe shrinkage of the binary orbit. We refer readers to see [Ivanova et al. \(2013\)](#) for a comprehensive review.

¹⁹ NS natal-kicks can also be called SN-kicks. Many studies of pulsar scale heights ([Gunn & Ostriker 1970](#)), proper motions of pulsars ([Cordes et al. 1993](#); [Lyne & Lorimer 1994](#); [Hobbs et al. 2005](#); [Verbunt et al. 2017](#)), and high velocities of some single NSs ([Chatterjee et al. 2005](#); [Becker et al. 2012](#)) have suggested that a kick should be imparted to the NS during core-collapse SNs.

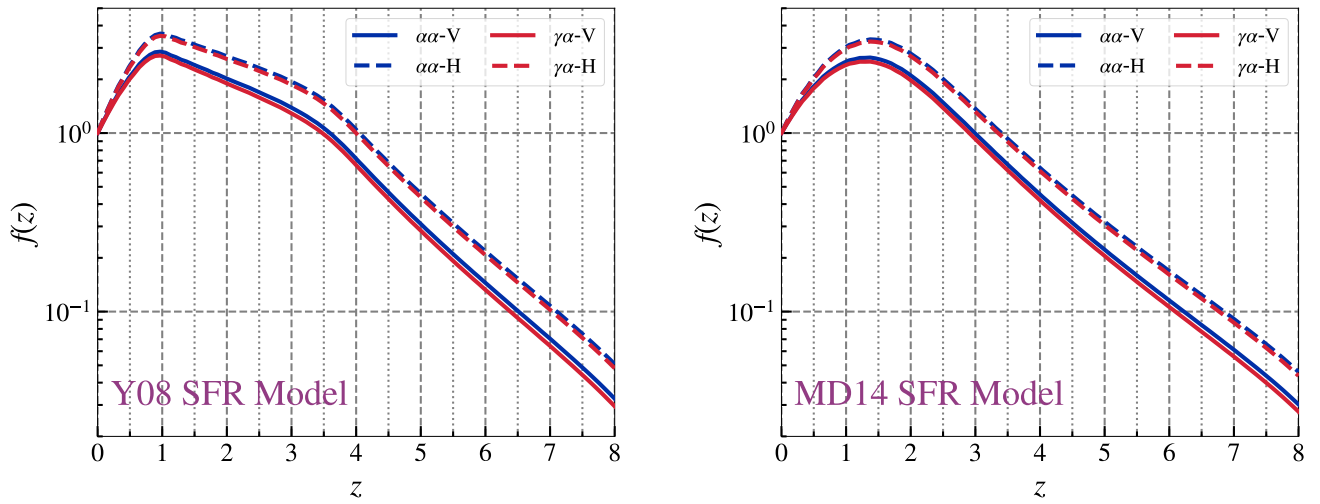


Figure A1. Redshift distributions of $f(z)$ derived from the method of convolution by Equation (A2). The Y08 SFR model is adopted in the left plot, while the MD14 model is applied in the right plot. The coloured solid lines and dashed lines denote different DTD models. The redshift cutoff $z = 8$ is adopted here.

Table A2. Technical information for some wide-field optical survey projects from [Zhu et al. \(2021, 2023\)](#). Note that a 300-s exposure time is adopted for the search limiting magnitude m^* in the three most common filters (g, r, i). The references are: (1) [Masci et al. \(2019\)](#), [Bellm et al. \(2019\)](#); (2) [Abell et al. \(2009\)](#), [Ivezic et al. \(2019\)](#); (3) [Shi et al. \(2018\)](#), [Wang et al. \(2023b\)](#); (4) [Yuan et al. \(2020\)](#); (5) [Gong et al. \(2019\)](#).

| Survey | m^*/mag | | | FoV/deg ² | Sky Coverage/deg ² | Reference |
|----------|------------------|------|------|----------------------|-------------------------------|-----------|
| | g | r | i | | | |
| ZTF | 21.6 | 21.3 | 20.9 | 47.7 | 30000 | (1) |
| LSST | 26.2 | 25.7 | 25.8 | 9.6 | 20000 | (2) |
| WFST | 24.2 | 24.0 | 23.3 | 6.55 | 20000 | (3) |
| Mephisto | 24.2 | 23.9 | 23.4 | 3.14 | 26000 | (4) |
| CSST | 26.3 | 26.0 | 25.9 | 1.1 | 17500 | (5) |